Red photoluminescence due to energy transfer from Eu^{2+} to Cr^{3+} in $Sr_3Al_{10}SiO_{20}$–$SrAl_{12}O_{19}$ mixed phases

2008 J. Phys. D: Appl. Phys. 41 065104

(http://iopscience.iop.org/0022-3727/41/6/065104)

J. Phys. D: Appl. Phys. **41** (2008) 065104 (7pp) doi:10.1088/0022-3727/41/6/065104

Red photoluminescence due to energy transfer from Eu^{2+} to Cr^{3+} in $Sr_3Al_{10}SiO_{20}$–$SrAl_{12}O_{19}$ mixed phases

Ruixia Zhong[1,3], Jiahua Zhang[1,4], Xia Zhang[1], Shaozhe Lu[1], Xinguang Ren[1] and Xiao-jun Wang[1,2]

[1] Key Laboratory of Excited State Processes, Changchun Institute of Optics, Fine Mechanics and Physics, Chinese Academy of Sciences, 16 Eastern South Lake Road, Changchun 130033, People's Republic of China
[2] Department of Physics, Georgia Southern University, Statesboro, GA 30460, USA
[3] Graduate School of Chinese Academy of Sciences, Beijing 100039, People's Republic of China

E-mail: zjiahua@public.cc.ji.cn (J.Zhang)

Received 12 November 2007, in final form 3 January 2008
Published 26 February 2008
Online at stacks.iop.org/JPhysD/41/065104

Abstract

$Sr_3Al_{10}SiO_{20}$–$SrAl_{12}O_{19}$, doped with Eu^{2+}, Cr^{3+} and (Eu^{2+} + Cr^{3+}) is prepared by solid-state reaction and energy transfer from Eu^{2+} to Cr^{3+} in the phase of $Sr_3Al_{10}SiO_{20}$ is the focus of investigation. The spectrum of $Sr_3Al_{10}SiO_{20}$–$SrAl_{12}O_{19}$: Eu^{2+} shows f–d emission bands at 460 and 400 nm. Cr^{3+} doped $Sr_3Al_{10}SiO_{20}$–$SrAl_{12}O_{19}$ yields emission lines at 688 and 696 nm and a broad emission band between 650 and 750 nm. The photoluminescence study and fluorescence lifetime measurements demonstrate efficient energy transfer from Eu^{2+} to Cr^{3+} in $Sr_3Al_{10}SiO_{20}$: Eu^{2+}, Cr^{3+}. The emission lines peak at 688 nm and 696 nm, which, respectively, originate from ^2E–$^4A_2$ transitions in the phases of $SrAl_{12}O_{19}$ and $Sr_3Al_{10}SiO_{20}$. The broad emission band of Cr^{3+} between 650 and 750 nm in the phase of $Sr_3Al_{10}SiO_{20}$ is considered to be the $^4T_2$–$^4A_2$ transition by calculating the strength of the octahedral crystal field Dq, the Racah parameters *B* and *C* as well as by constructing the Tanabe–Sugano diagram.

1. Introduction

Much attention has been paid to the development of advanced luminescent materials for applications such as flat panel displays, Hg-free lamps and x-ray imaging systems. Among the various types of flat panel displays are plasma display panels, which have a competitive edge in the large-screen display market [1–3]. Kubota *et al* have reported a new luminescent host, $Sr_3Al_{10}SiO_{20}$, for application in FEDs [4]. $Sr_3Al_{10}SiO_{20}$: Tb^{3+} shows efficient green emission under vacuum ultraviolet (VUV) excitation, the relative intensity of which is higher than that of other Tb^{3+}-doped strontium aluminium silicates, e.g. $Sr_2Al_2SiO_7$ and $SrAl_2Si_2O_8$ as well as $SrAl_{12}O_{19}$ [5]. Similarly, a moderately efficient blue emission is obtained from $Sr_3Al_{10}SiO_{20}$: Eu^{2+} with a relative intensity of 60% of commercial phosphor $BaMgAl_{10}O_{17}$: Eu^{2+} (BAM) under VUV excitation [6]. However, red phosphor for the new luminescent host of $Sr_3Al_{10}SiO_{20}$ is absent.

As we know, the Cr^{3+} ion with red emission is one of the most used activators for solid-state laser [7,8] and luminescent materials [9]. Recently, we have reported the efficient energy transfer from Eu^{2+} to Cr^{3+} in $Sr_4Al_{14}O_{25}$ [10,11] and $SrAl_{12}O_{19}$ [12]. Hence, our experiments are extended to study the energy transfer processes in Eu^{2+}, Cr^{3+} co-doped $Sr_3Al_{10}SiO_{20}$.

In this paper, we report the photoluminescence characteristics of $Sr_3Al_{10}SiO_{20}$-$SrAl_{12}O_{19}$: Eu^{2+}, Cr^{3+}. The energy transfer from Eu^{2+} to Cr^{3+} and the deep red emission of Cr^{3+} have been studied in the phase of $Sr_3Al_{10}SiO_{20}$: Eu^{2+}, Cr^{3+}. It is found that sharp emission lines peak at 688 nm and 696 nm which, respectively, originate from the ^2E–$^4A_2$ transitions in the phases of $SrAl_{12}O_{19}$ and $Sr_3Al_{10}SiO_{20}$. A broad band between 650 and 750 nm is also found which is considered to be the $^4T_2$–$^4A_2$ transition by the comparison of luminescence at room temperature with that at 77 K as well as the construction of the Tanabe–Sugano diagram.

[4] Author to whom any correspondence should be addressed.

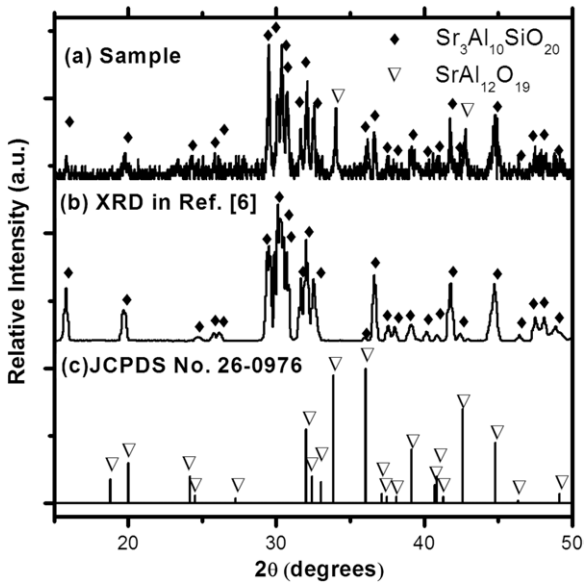

Figure 1. XRD patterns of our sample, $Sr_3Al_{10}SiO_{20}$–$SrAl_{12}O_{19}$: Eu^{2+}, Cr^{3+}, the standard $Sr_3Al_{10}SiO_{20}$ pattern in [6] and the standard $SrAl_{12}O_{19}$ pattern (JCPDS-No 26-0976).

2. Experiments

Samples of $Sr_3Al_{10}SiO_{20}$–$SrAl_{12}O_{19}$: Eu^{2+}, Cr^{3+} have been synthesized by high temperature solid-state reaction. The starting materials are $SrCO_3$ (AR), Al_2O_3 (AR), Eu_2O_3 (99.9%), Dy_2O_3 (99.9%), SiO_2 (AR), Cr_2O_3 (AR) and H_3BO_3 (AR). The powder samples have been weighed according to the molar ratio given by the formula. All mixtures are grounded for 1 h, then preheated at 1000 °C in air for 4 h and finally sintered at 1450 °C in a reducing atmosphere for 7 h.

Emission and excitation spectra are measured with a Hitachi F-4500 Spectra-fluorometer. In fluorescence lifetime measurements, the fourth (266 nm) harmonic of a Nd–YAG laser (Spectra-Physics, GCR 130) is used as an excitation source, and the signal is detected with a Tektronix digital oscilloscope model (TDS 3052). The crystalline structure of the sample is investigated by x-ray diffraction (XRD), using a Siemens D-500 equipment with a Cu target radiation source.

3. Results and discussion

XRD patterns of our sample $Sr_3Al_{10}SiO_{20}$–$SrAl_{12}O_{19}$: Eu^{2+}, Cr^{3+}, the standard $Sr_3Al_{10}SiO_{20}$ pattern in [6] and the standard $SrAl_{12}O_{19}$ pattern (JCPDS-No 26-0976) are shown in figure 1. The XRD peaks of our sample $Sr_3Al_{10}SiO_{20}$–$SrAl_{12}O_{19}$: Eu^{2+}, Cr^{3+} match well with the standard $Sr_3Al_{10}SiO_{20}$ pattern except for two peaks: one peaks at 34° and another peaks at 42°, which belongs to the second phase, $SrAl_{12}O_{19}$. The pure $Sr_3Al_{10}SiO_{20}$ phase is composed of one-dimensional pillars of edge-sharing AlO_6 octahedra and six-member rings of corner-sharing (Al, Si)O_4. The structure is unique and has not been previously observed among luminescent aluminium-based oxides. The composition $Sr_3Al_{10}SiO_{20}$ is in the monoclinic system in a space group of $C2/m$.

Figure 2 shows the excitation and emission spectra of $Sr_3Al_{10}SiO_{20}$–$SrAl_{12}O_{19}$: 1% Eu^{2+} (*a*), $Sr_3Al_{10}SiO_{20}$–$SrAl_{12}O_{19}$: 1% Cr^{3+} (*b*), $SrAl_{12}O_{19}$: 1% Eu^{2+} (*c*) and $SrAl_{12}O_{19}$: 1% Cr^{3+} (*d*). Both emission and excitation spectra of Eu^{2+} in $Sr_3Al_{10}SiO_{20}$–$SrAl_{12}O_{19}$: 1% Eu^{2+} (figure 2(*a*)) are broad bands, which can be assigned to 5d–4f transition of Eu^{2+}. The emission spectra of Eu^{2+} in $Sr_3Al_{10}SiO_{20}$–$SrAl_{12}O_{19}$: 1% Eu^{2+} consists of two bands: the main peak centres at 460 nm named Eu1 and the shoulder peak centres at 400 nm named Eu2. The excitation spectra of Eu1 and Eu2 are different. It means there exist two different emitting centres which can be from different environments in one phase or from two different phases. Comparing the emission and excitation spectra in figure 2(*a*) with those in figure 2(*c*), it is worth noting that the emission and excitation spectra of the Eu2 centre in $Sr_3Al_{10}SiO_{20}$–$SrAl_{12}O_{19}$ are the same as that in $SrAl_{12}O_{19}$ [12]. It indicates that the emission band centred at 400 nm is from the f–d transition in the phase of $SrAl_{12}O_{19}$. There is only one emitting centre of Eu in pure $Sr_3Al_{10}SiO_{20}$: 1% Eu^{2+} which peaks at 460 nm. As shown in figure 2(*b*), the emission lines peaking at 688 and 696 nm as well as a broad band appearing between 650 and 750 nm comprise the emission spectra of Cr^{3+} ions in $Sr_3Al_{10}SiO_{20}$–$SrAl_{12}O_{19}$. However, not all peaks appearing in the emission spectra in figure 2(*b*) are from pure $Sr_3Al_{10}SiO_{20}$. As shown in figure 2(*d*), the emission spectra of Cr^{3+} in pure $SrAl_{12}O_{19}$ consist of only one peak at 688 nm whose excitation spectra are the same as those of the 688 nm emitting centre in $Sr_3Al_{10}SiO_{20}$–$SrAl_{12}O_{19}$ [12]. It means that the emission lines at 688 nm in the emission spectra in figure 2(*b*) are from the phase of $SrAl_{12}O_{19}$. Thus, only the emission line at 696 nm and the broad band between 650 and 750 nm comprise the emission spectra of Cr^{3+} in the pure phase of $Sr_3Al_{10}SiO_{20}$. The difference in the excitation spectra between the 688 nm emission line and the 696 nm emission line also indicates that the environment of the 688 nm emitting centre is different from that of the 696 nm emitting centre.

The energy transfer from Eu^{2+} to Cr^{3+} in the phase of $SrAl_{12}O_{19}$ has been discussed in detail in [12], so we will focus on the discussion on energy transfer in the phase of $Sr_3Al_{10}SiO_{20}$ in this paper.

Figure 3 depicts the emission and excitation spectra of $Sr_3Al_{10}SiO_{20}$–$SrAl_{12}O_{19}$: x% Eu^{2+}, 1% Cr^{3+} (x = 0, 0.05, 0.1, 0.5, 1, 2). In $Sr_3Al_{10}SiO_{20}$–$SrAl_{12}O_{19}$: x% Eu^{2+}, 1% Cr^{3+}, both ^2E–$^4A_2$ emissions of Cr^{3+} at 696 nm and broad emission bands are observed under 320 nm excitation. The origin of the broad band emission of Cr^{3+} ions is discussed later. The excitation spectra of the 696 nm emissions consist of $^4A_2$–$^4T_1$ (F) absorption at 406 nm and $^4A_2$–$^4T_2$ (F) absorption at 587 nm of Cr^{3+} and f–d absorption of Eu^{2+} in the ultraviolet region. The intensities of the 587 nm excitation bands are normalized. From figure 3, the 460 nm emission band of Eu^{2+} has spectral overlaps with the absorption bands of Cr^{3+}, indicating the possibility of energy transfer from Eu^{2+} to Cr^{3+}. It can also be seen that the excitation bands originating from f–d transition of Eu^{2+} in the ultraviolet region grow up with the increase in Eu^{2+} concentrations when only the red emission at 696 nm of Cr^{3+} is monitored until the Eu^{2+} concentration is up to 1%. Furthermore, the red emission of Cr^{3+} increases with

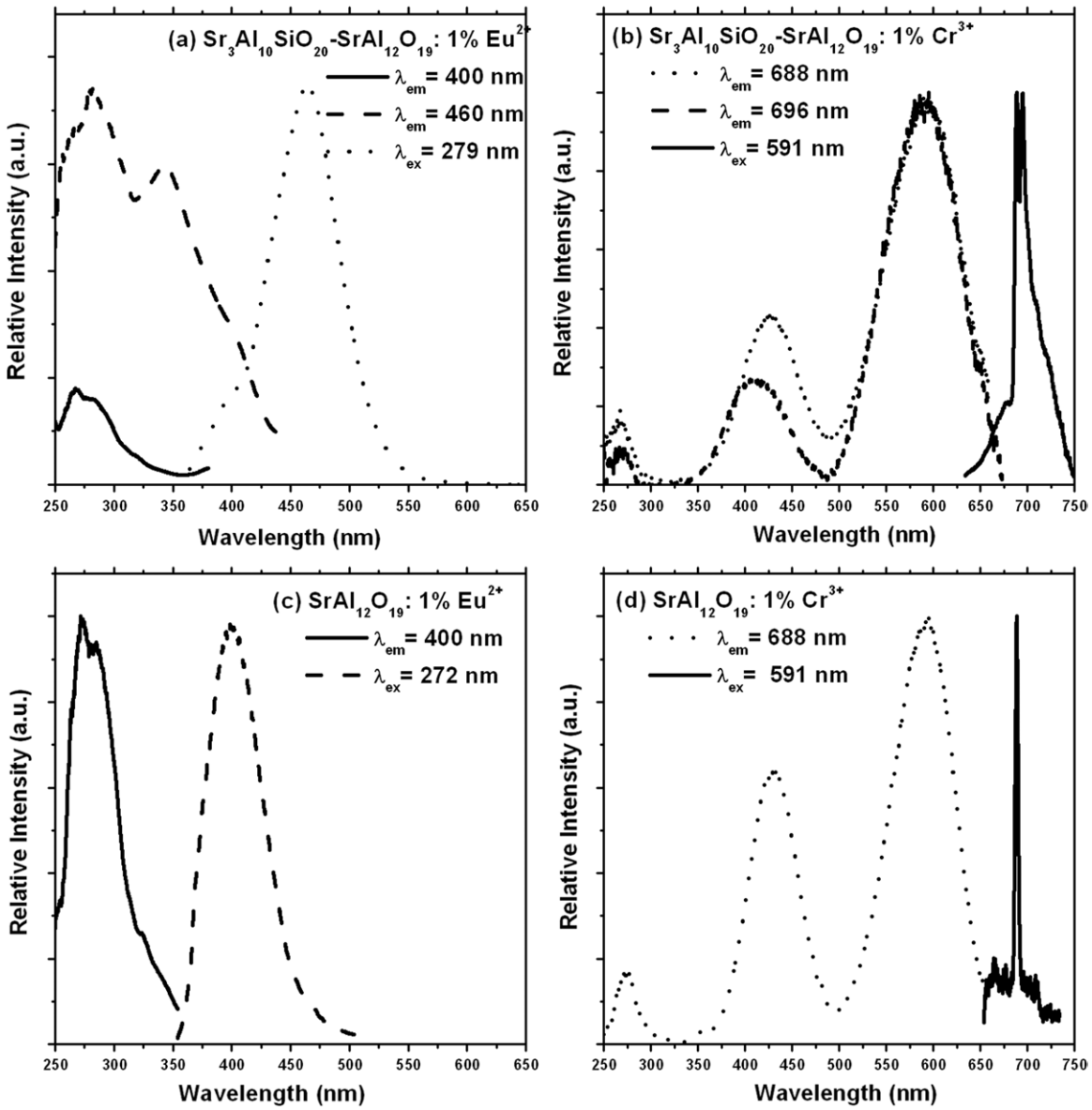

Figure 2. Excitation and emission spectra of $Sr_3Al_{10}SiO_{20}$–$SrAl_{12}O_{19}$: 1% Eu^{2+} (*a*), $Sr_3Al_{10}SiO_{20}$–$SrAl_{12}O_{19}$: 1% Cr^{3+} (*b*), $SrAl_{12}O_{19}$: 1% Eu^{2+} (*c*) and $SrAl_{12}O_{19}$: 1% Cr^{3+} (*d*).

the increase in Eu^{2+} concentrations under 320 nm excitation, by which only Eu^{2+} can be excited because there is no absorption of Cr^{3+} at this wavelength as shown in figure 3. These results strongly indicate the performance of energy transfer from Eu^{2+} to Cr^{3+} in $Sr_3Al_{10}SiO_{20}$: Eu^{2+}, Cr^{3+}.

Figure 4 shows the emission spectra of $Sr_3Al_{10}SiO_{20}$–$SrAl_{12}O_{19}$: 1% Eu^{2+}, *x*% Cr^{3+} (x = 0.5, 1, 2, 3, 4 and 5) under 320 nm excitation, where the intensities of the blue bands at 460 nm are normalized. When maintaining the Eu^{2+} concentration and increasing the Cr^{3+} contents up to 5%, the red lines at 696 nm and the broad bands from Cr^{3+} are enhanced, indicating the increase in energy transfer efficiency since Cr^{3+} cannot be excited by 320 nm directly. The addition of Cr^{3+} ions leads to an increase in Cr^{3+} surrounding the Eu^{2+} ion, thus resulting in more efficient energy transfer. As we know, the concentration of Cr^{3+} does not affect the change of phases in this system. Thus, the ratio of the number of Eu1 to the number of Eu2 can be considered as a constant. From the emission spectra in figure 4, the emission band from the Eu2 centre increases relatively to the Eu1 centre, while the emission line at 688 nm decreases relatively to the 696 nm emission. It means the ratio of the red emission to the blue one in the phase of $Sr_3Al_{10}SiO_{20}$ grows more rapidly than that in the phase of $SrAl_{12}O_{19}$. It indicates that the energy transfer rate in $Sr_3Al_{10}SiO_{20}$ is faster than that in $SrAl_{12}O_{19}$. According to the emission spectra shown in figure 4, the intensity ratios of the red emission of Cr^{3+} to the blue emission of Eu^{2+} are plotted as a function of Cr^{3+} concentrations, as shown in figure 5. The ratio grows with increasing Cr^{3+} concentration. It means that the blue emission can be partly converted to the red one and the ratio of the red to the blue can be controllable by changing the concentration of Eu and Cr.

In order to analyse the energy transfer rate and efficiency as a function of Cr^{3+} concentration, the fluorescence decay

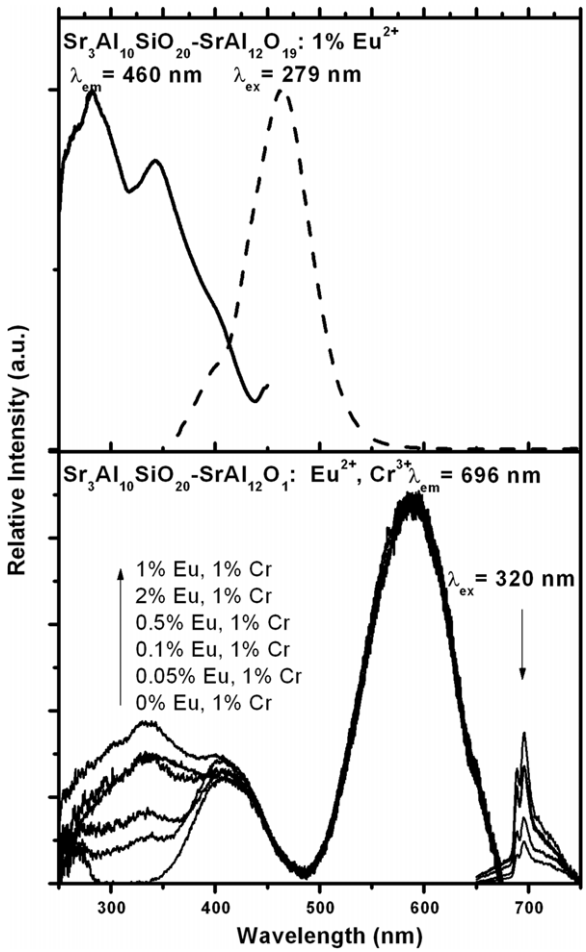

Figure 3. Emission and excitation spectra of $Sr_3Al_{10}SiO_{20}$–$SrAl_{12}O_{19}$: 1% Eu^{2+} and $Sr_3Al_{10}SiO_{20}$–$SrAl_{12}O_{19}$: x% Eu^{2+}, 1% Cr^{3+} (x = 0, 0.05, 0.1, 0.5, 1, 2), where the intensities of the 587 nm absorption bands are normalized.

curves of 460 nm emissions originating from Eu^{2+} in the phase of $Sr_3Al_{10}SiO_{20}$ doped with 1% Eu^{2+}, x% Cr^{3+} (x = 0.5, 1, 2, 3, 4 and 5) are measured and presented in figure 6. As we know, if the average donor–acceptor transfer rate is larger than the donor–donor diffusion rate, the donors will depart from single exponential decay [13, 14]. Thus, the decay patterns shown in figure 6 slightly depart from single exponential function at the high concentration of Cr^{3+}. According to the Inokuti–Hirayama model, the lifetime can be obtained by the following definition [15]:

$$\tau = \frac{1}{I_0}\int_0^\infty I(t)\,\mathrm{d}t, \tag{1}$$

where I_0 is the fluorescence intensity at the time of $t = 0$. According to equation (1), the lifetimes of Eu^{2+} in the phase of $Sr_3Al_{10}SiO_{20}$ at different Cr concentrations are shown in figure 6 (inset). The lifetimes of Eu^{2+} (τ_{blue}) reduce with increasing Cr^{3+} concentration because of the energy transfer from Eu^{2+} to Cr^{3+}. As is known, the macroscopic energy transfer rate W_{Eu-Cr} as a function of Cr^{3+} concentration can be evaluated from the lifetime measurement since

$$W_{Eu-Cr} = 1/\tau_{blue} - 1/\tau_{blue,0}, \tag{2}$$

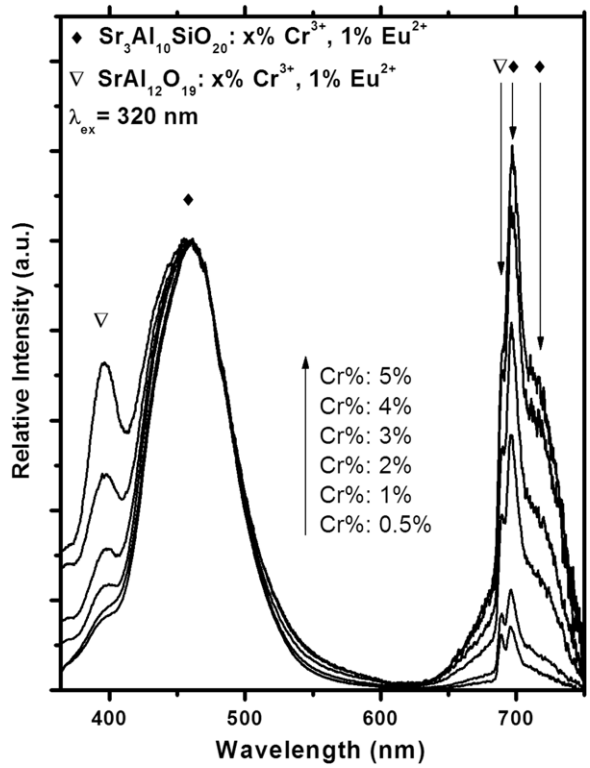

Figure 4. Emission spectra of $Sr_3Al_{10}SiO_{20}$–$SrAl_{12}O_{19}$: 1% Eu^{2+}, x% Cr^{3+} (x = 0.5, 1, 2, 3, 4 and 5) under 320 nm excitation, where the intensities of the blue bands at 460 nm are normalized.

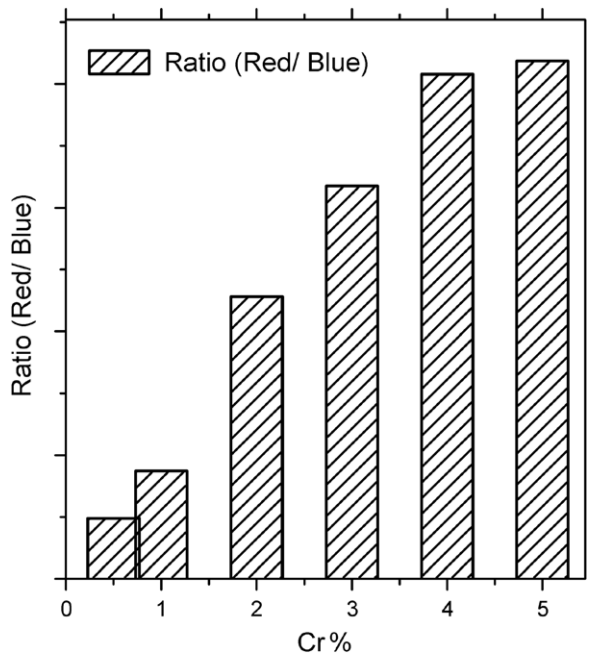

Figure 5. Dependence of the ratio for the red emission to the blue one on the Cr^{3+} concentration.

where $\tau_{blue,0}$ is the intrinsic decay lifetime of Eu^{2+}. When the concentration of Cr^{3+} is low, the energy transfer rate is too small to be ignored. Thus, the lifetime of Eu^{2+} in $Sr_3Al_{10}SiO_{20}$–$SrAl_{12}O_{19}$: 1% Eu^{2+}, 0.5% Cr^{3+} can be recognized as the intrinsic decay lifetime. According to

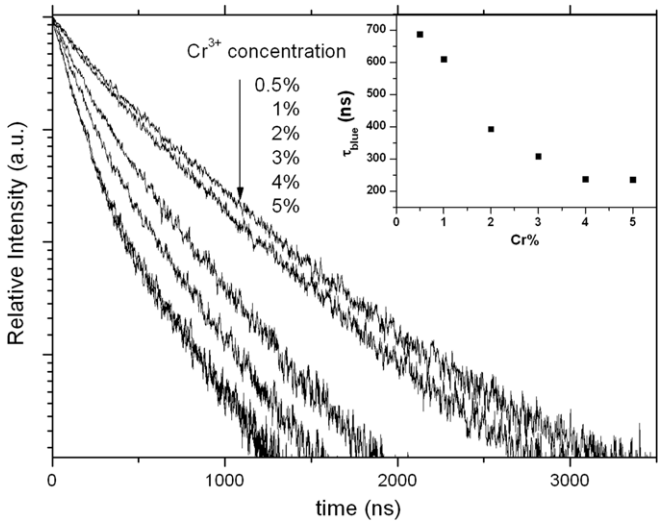

Figure 6. The fluorescence decay curves of 460 nm (τ_{blue}) emissions for different Cr^{3+} concentrations. The lifetimes of Eu^{2+} in the phase of $Sr_3Al_{10}SiO_{20}$ at different Cr concentrations are given in the inset.

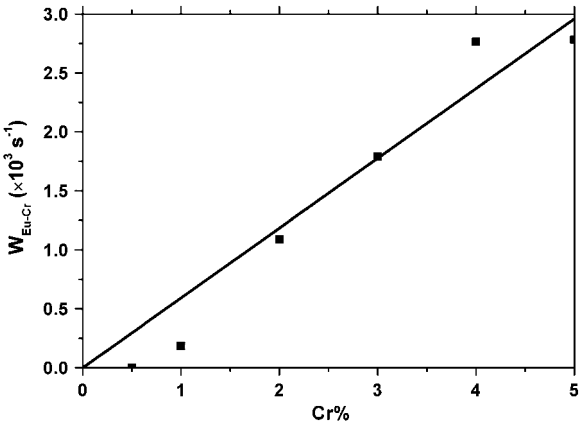

Figure 7. Dependence of the energy transfer rate on the Cr^{3+} concentration.

equation (2), the energy transfer rate has been obtained and shown in figure 7. The energy transfer rate between Eu and Cr is considered to be a linear relationship with the Cr concentration, described as a function of $W_{Eu-Cr} = aC_{Cr}$, where C_{Cr} is the Cr^{3+} concentration; a is the constant for the energy transfer rate. The calculated curves are also shown in figure 7. The value of a is 5.9×10^7 ($s^{-1}\,mol^{-1}$). The calculated curve perfectly agrees with the experimental data. The energy transfer rate increases following the Cr^{3+} concentration. The enhancement of the number of Cr ions surrounding the Eu ions leads to a short distance between Eu and Cr, so the energy transfer rate becomes fast.

The energy transfer efficiency (η_T) as a function of Cr^{3+} is also investigated. According to the definition suggested by Paulous [16], η_T can be expressed by

$$\eta_T = 1 - \frac{\tau_{blue}}{\tau_{blue,0}}. \tag{3}$$

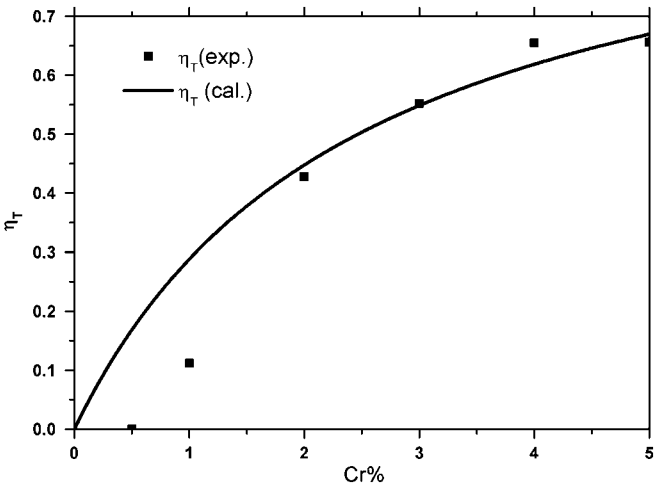

Figure 8. Dependence of the energy transfer efficiency on the Cr^{3+} concentration.

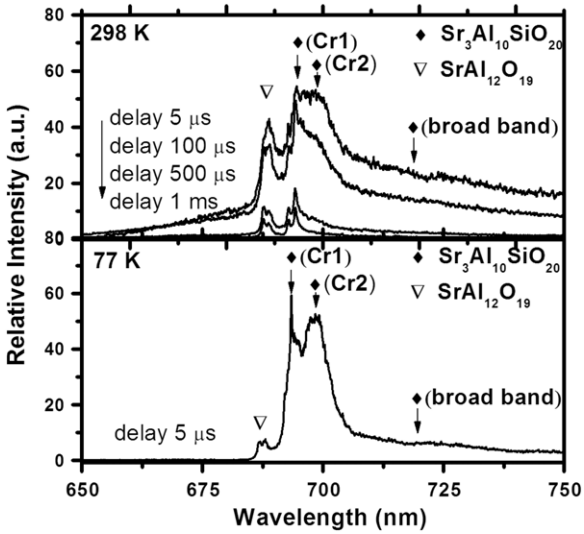

Figure 9. Time-resolved emission spectra at 298 and 77 K of $Sr_3Al_{10}SiO_{20}$–$SrAl_{12}O_{19}$: Eu^{2+}, Cr^{3+}.

Using equation (3) and the measured lifetimes, the energy transfer efficiency has been obtained and shown in figure 8. The calculated curves in figure 8 are shown according to the relationship between the energy transfer rate (W_{Eu-Cr}) and energy transfer efficiency (η_T) expressed by

$$\eta_T = 1 - \frac{1}{a\tau_{blue,0}C_{Cr} + 1}. \tag{4}$$

The calculated curves perfectly agree with the experimental data. With increasing Cr^{3+} concentration, the transfer efficiency in the $Sr_3Al_{10}SiO_{20}$ phase increases.

To make clear the origin of the broad emission band, time-resolved emission spectra of $Sr_3Al_{10}SiO_{20}$–$SrAl_{12}O_{19}$: Eu^{2+}, Cr^{3+} at 298 and 77 K are shown in figure 9. It is obvious that room temperature recorded spectra are characterized by three emission lines and a broad band. The emission lines are, respectively, located at 688 nm, 694 nm and 696 nm. The 688 nm emission originates from the ^2E–$^4A_2$ transition in the

phase of $SrAl_{12}O_{19}$ as we have discussed above. The 694 and 696 nm emissions are from the ^2E–$^4A_2$ transition of Cr^{3+} with different environments in the phase of $Sr_3Al_{10}SiO_{20}$. According to [17], two non-equivalent octahedral sites of AlO_6 exist in the phase of $Sr_3Al_{10}SiO_{20}$. When the Cr ions replace the Al ions, two non-equivalent sites of Cr1 and Cr2 exist. Thus, the two R lines originating from Cr1 and Cr2 sites are, respectively, observed at 694 nm and 696 nm in the high-resolved emission spectra. As shown in figure 9, the emission line at 696 nm and the broad emission band have the same decay tendency and decay fast compared with the 694 nm emission. Both the 696 nm emission and the broad band disappeared in the spectra recorded after delaying by 1 ms. It is apparent that the spectrum recorded at 77 K only consists of the ^2E–$^4A_2$ transitions from the Cr ions in the phase of $SrAl_{12}O_{19}$ and Cr1 and Cr2 in the phase of $Sr_3Al_{10}SiO_{20}$. The broad band becomes weak. Therefore, the broad emission band is considered to be the $^4T_2$–$^4A_2$ transition of the Cr^{3+} ions located at the weak crystal field. The thermal population of the $^4T_2$ state is from the ^2E state. Thus, the emission band of $^4T_2$–$^4A_2$ transition becomes weak at 77 K.

As we know, the spectroscopic properties of Cr^{3+} system depend directly on the crystal field strength (Dq/B) which determines the sequence of the two excited states, the ^2E doublet and $^4T_2$ quartet. Since the $^4T_2$ quartet is sensitive to Dq/B and the ^2E doublet, in contrast, is insensitive to Dq/B, their energy separation, $\Delta = E(^4T_2)$–$E(^2E)$, varies in different systems. The energy separation Δ has a decisive effect on the Cr^{3+} emission. When $\Delta < 0$, the low field case, Cr^{3+} luminescence arises from the spin-allowed $^4T_2 \rightarrow {}^4A_2$ transition and is characterized by a broad band with a short lifetime. In the high field case,$\Delta > 0$, the Cr^{3+} luminescence arises from the spin-forbidden $^2E \rightarrow {}^4A_2$ transition and is characterized by sharp *R*lines with long lifetime. In intermediate fields, $|\Delta| \rightarrow 0$, the ^2E and $^4T_2$ states strongly couple both thermally and through spin–orbit coupling. As a consequence, the luminescence will have characteristics of both states. Thus, that both emissions originating from $^4T_2$ and ^2E states have been observed in the emission spectra means the energy separation Δ in the phase of $Sr_3Al_{10}SiO_{20}$ is small. The strength of the octahedral crystal field Dq/B and the Racah parameters B and C are calculated from the excitation spectra of R lines shown in figure 2. It is well known that Dq is obtained directly from the energy corresponding to the peak of the $^4A_2$–$^4T_2$ absorption band, which is equal to 10 Dq,

$$\mathrm{Dq} = [E(^4T_2) - E(^4A_2)]/10. \tag{5}$$

Considering ΔE as the energy difference between $^4T_2$ and the lowest $^4T_1$ state, which experimentally is the separation between the strong absorption bands in figure 2(*b*), the B value is obtained from

$$\frac{B}{\mathrm{Dq}} = \frac{\left(\frac{\Delta E}{\mathrm{Dq}}\right)^2 - 10\frac{\Delta E}{\mathrm{Dq}}}{15\left(\frac{\Delta E}{\mathrm{Dq}} - 8\right)}. \tag{6}$$

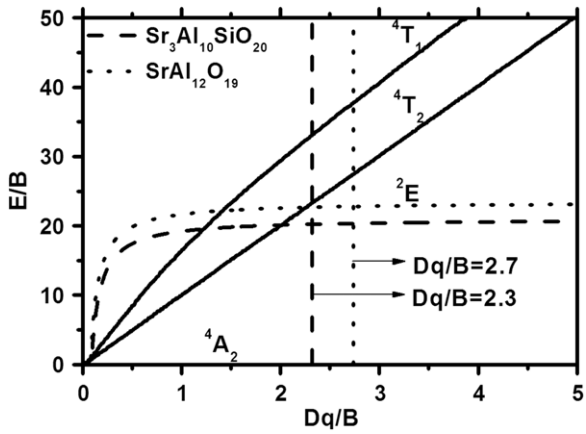

Figure 10. Tanabe–Sugano diagram constructed for the Cr^{3+} site in the phase of $Sr_3Al_{10}SiO_{20}$ and $SrAl_{12}O_{19}$. The dashed line and the dotted line are, respectively, the approximation for the ^2E level of $Sr_3Al_{10}SiO_{20}$ and $SrAl_{12}O_{19}$ given by equation (4).

The last Racah's parameter can be calculated from an approximate expression given by Henderson and Imbusch [18]:

$$C = [E(^2E) - 7.9B + 1.8B^2/\mathrm{Dq}]/3.05. \tag{7}$$

The Tanabe–Sugano diagram constructed for the Cr^{3+} site in the phase of $SrAl_{12}O_{19}$ and $Sr_3Al_{10}SiO_{20}$ is given in figure 10. The vertical lines represent the appropriate value for Dq/B (2.7 for $SrAl_{12}O_{19}$; 2.3 for $Sr_3Al_{10}SiO_{20}$). In this figure we have also included the exact solution for the ^2E state calculated from equation (6) (dashed line, $Sr_3Al_{10}SiO_{20}$; dotted line, $SrAl_{12}O_{19}$). From the diagram, the ^2E states correspond to the lowest excited energy level and the energy difference between $^4T_2$ and ^2E is 2188 cm^{-1} for $Sr_3Al_{10}SiO_{20}$ and 3157 cm^{-1} for $SrAl_{12}O_{19}$. Thus, the electrons on the ^2E level can be excited to the $^4T_2$ level even at room temperature in the phase of $Sr_3Al_{10}SiO_{20}$. Thus, the broad emission band from $^4T_2$–$^4A_2$ transition can be observed in the phase of $Sr_3Al_{10}SiO_{20}$. However, the crystal field of $SrAl_{12}O_{19}$ is strong. The energy difference between $^4T_2$ and ^3E is so large that the electrons on the ^2E level cannot be excited to the $^4T_2$ level at the room temperature. Therefore, the broad emission band from the $^4T_2$–$^4A_2$ cannot be observed in the phase of $SrAl_{12}O_{19}$. In figure 9, it is apparent that the Cr emissions originating from $^4T_2$–$^4A_2$ transition and ^2E–$^4A_2$ transition of Cr2 ions in $Sr_3Al_{10}SiO_{20}$ have short lifetimes. As we know, the ^2E state has a long lifetime. The short lifetime for ^2E–$^4A_2$ transition of Cr2 ions in $Sr_3Al_{10}SiO_{20}$ is because of the interaction between $^4T_2$ and ^2E states. The thermal population of the $^4T_2$ state is from the ^2E state. The population between $^4T_2$ and ^2E states is dynamic thermal equilibrium. Thus, the lifetime of ^2E state is as short as that of the $^4T_2$ state.

As discussed above, the Cr ions in the phase of $Sr_3Al_{10}SiO_{20}$ give the sharp line from ^2E–$^4A_2$ transition and the broad band from $^4T_2$–$^2A_2$ transition. The interaction between $^4T_2$ and ^2E states makes the lifetime of the ^2E state short. The energy transfer from Eu^{2+} to Cr^{3+} occurs in co-doped samples. Compared with the phase of $SrAl_{12}O_{19}$, the energy transfer rate is fast in the phase of $Sr_3Al_{10}SiO_{20}$.

4. Conclusions

In summary, energy transfer has been observed in the phase of $Sr_3Al_{10}SiO_{20}$ with Eu, Cr co-doped, which leads to the following results: (1) the intensity of the red emission of Cr^{3+} is enhanced by increasing the concentration of optically excited Eu^{2+} and (2) as the concentration of Eu^{2+} is fixed, the ratio of the red emission to the blue of Eu^{2+} increases with increasing Cr^{3+} concentration when only Eu^{2+} is optically excited. The energy transfer rate and efficiency increase following the Cr^{3+} concentration. Therefore, the red emission can be obtained by converting the blue emission from Eu^{2+}. In addition, both the R line from ^2E–$^4A_2$ transition and the broad emission band from $^4T_2$–$^2A_2$ transition have been observed in the phase of $Sr_3Al_{10}SiO_{20}$. The reason is that the crystal field for the Cr^{3+} ions in $Sr_3Al_{10}SiO_{20}$ is weak ($Dq/B = 2.3$). The difference between $^4T_2$ and ^2E states is 2188 cm^{-1} which allows the electrons on the ^2E level excite to the $^4T_2$ level even at the room temperature. Thus, both the R line and the broad emission band appear in the emission spectra of Cr ions. The small difference between $^4T_2$ and ^2E states also makes the interaction between $^4T_2$ and ^2E states strong which results in the short lifetime of ^2E states.

Acknowledgments

This work is financially supported by the MOST of China (2006CB601104, 2006AA03A138) and the National Nature Science Foundation of China (10774141, 10574128).

References

[1] Justel T, Nikol H and Ronda C 1998 *Angew. Chem. Int. Edn* **37** 3084
[2] Blasse G and Grabmaier B C 1994 *Luminiscent Materials* (Berlin: Springer)
[3] Wang J, Yoo Y, Gao C, Takeuchi I, Sun X, Chang H, Xiang X D and Schults G 1998 *Science* **279** 1712
[4] Kubota S, Yamane H and Shimada M 2001 *Acta Crystallogr.* E **57** 60
[5] Kubota S, Yamane H and Shimada M 2002 *Chem. Mater.* **14** 4015
[6] Kubota S, Yamane H and Shimada M 2002 *Appl. Phys. Lett.* **81** 2749
[7] Qui Y 1993 *J. Phys.: Condens. Matter* **5** 2041
[8] Kaminskii A A 1996 *Crystalline Lasers: Physical Processes and Operating Schemes* (Boca Raton, FL: CRC Press)
[9] Geusic J E, Marcos H M and Van Uitert L G 1964 *Appl. Phys. Lett.* **4** 182
[10] Zhong R X, Zhang J H, Zhang X, Lu S Z and Wang X J 2006 *J. Lumin.* **119–20** 327
[11] Zhong R X, Zhang J H, Zhang X, Lu S Z and Wang X J 2006 *Appl. Phys. Lett.* **88** 201916
[12] Zhong R X, Zhang J H, Zhang X, Lu S Z and Wang X J 2007 *Nanotechnology* **18** 445707
[13] Broer M M, Huver D L, Yen W M and Zwicker W K 1982 *Phys. Rev. Lett.* **49** 394
[14] Broer M M, Huver D L, Yen W M and Zwicker W K 1984 *Phys. Rev.* B **29** 2382
[15] Inokuti M and Hirayama F 1965 *J. Chem. Phys.* **43** 1978
[16] Paulose P I, Jose G, Thomas V, Unnikrishnan N V and Warrier M K R 2003 *J. Phys. Chem. Solids* **64** 841
[17] Capron M, Fayon F, Coutures J, Massiot D and Douy A 2002 *J. Solid State Chem.* **169** 53–9
[18] Henderson B and Imbush G F 1989 *Optical Spectroscopy of Inorganic Solids* (Oxford: Oxford Science Publications)